bioresources.cnr.ncsu.edu

Enhanced Dimensional Stability of Straw-based Biocomposites Modified with UV Light-cured Coatings

Yuan Yuan,[a,b] Xiang Sun,[c] Dong Xu,[a,b] Jianyu He,[a,b] Xuansong Wang,[a,b] Donghua Wu,[a,b] and Sidan Li [a,b,*]

This study demonstrated an effective method to enhance the dimensional stability of straw-based biocomposites with modified lignosulfonate as a binder. The ultraviolet (UV) light-curable nanosol was prepared by adding 3-(trimethoxysilyl)propyl methacrylate (MEMO) as sol–gel precursor into polyvinyl alcohol (PVA) solution. The MEMO/PVA coatings were generated using 2-hydroxy-2-methyl-1-phenylpropan-1-one (Darocur 1173) as radical photo-initiator and chitosan (CS) as additive, on straw-based biocomposites *via* UV-curing process. The effects of the crucial steps, such as the UV-curing process, hydrolysis time, Darocur 1173 dosage, and CS dosage on the dimensional stability of straw-based biocomposites, were evaluated. The optimum preparation parameters, obtained using the Box–Behnken design, were 31.9 min hydrolysis time, 4.5% Darocur 1173 dosage, and 2.7% CS dosage. Moisture resistance of minimum TS of CS-MEMO/PVA-coated straw-based biocomposites resulted in ~23.1% reduction in dimensional stability without significant decline in the mechanical properties when compared with those without UV curing. Moreover, the glossy spherical particles underwent arrangement in a fish-scale shape with scales closely linked with each other and no agglomeration occurred in CS-MEMO/PVA hybrid film. The CS promoted the cross-linking of MEMO/PVA coating on the biocomposite surface. The resulting biocomposites can be directly applied to public humid-environment applications such as bath furniture and bathroom partitions.

INTRODUCTION

The dimensional stability of wood or non-wood composites is an important characteristic of consumer concern that demands comprehensive understanding (Okuda and Sato 2007; Yuan *et al.* 2014, 2019). Under normal circumstances, a waterproof barrier can be achieved by completely covering the surface of the composite board with a dense polymer layer or coating (Gao *et al.* 2023; Liu *et al.* 2023; Tao *et al.* 2023). The application of nanotechnology has been shown to improve the surface properties of materials, leading to their high durability. Among various methods involved in nanotechnology, the sol–gel technique can aid in customization of surface characteristics to a certain extent and

combine different functions into a single material in a convenient and cost-effective manner (Gao *et al.* 2015; Zhang and Guo 2023). Relevant studies on sol–gel process mainly have focused on functionalization of fiber or wood surfaces to improve their characteristics and impart new properties (Nkeuwa *et al.* 2014a,b; Wang *et al.* 2020). The nano-sol prepared using tetraethyl orthosilicate or γ-aminopropyl triethoxysilane was used as the precursor and applied to the surface of the treated material through impregnation and heat treatment to obtain good contact angle, and the surface of the treated material exhibited superhydrophobic properties (Li and Li 2018).

Corn stalk is approximately 90% cheaper than all other agricultural fibers used to date for preparation of composites (Shah 2013). The stalks left in the field are burned with the release of large amounts of smoke, which is already of major concern in northern China. In addition, from the perspective of sustainable development, the use of corn stalks is more advantageous than the use of some other natural fibers, such as jute, flax, and hemp, that require large land areas to grow (Luo *et al.* 2016).

Biocomposites possess a range of specialized structures with different requirements on temperature and operating conditions, which depend on their applications in different areas (Mathias *et al.* 2015; Noor Haris *et al.* 2022; Yavuz 2023). Therefore, surface hydrophobic modification is usually performed by surface coating method (Huang *et al.* 2021). Moreover, most adhesives and dispersants used in surface modification of biocomposites are organic solvents. These can cause environmental pollution, hindering the promotion and advancement of this process. Furthermore, volatile organic compounds (VOCs) are emitted from coating formulations, and their production cost is very high.

Ultraviolet (UV)-curing technology has emerged as an efficient alternative that is being developed rapidly (Ghazali *et al.* 2021; Dong *et al.* 2022). UV-cured coatings have high scratch and chemical resistances, involve VOC and waste reductions, and they are economical (high production speed with low footprint) (William *et al.* 2014). Surface coatings with desired functionalities can be obtained by layering the photocurable coatings on the substrate and curing them into films under UV irradiation (Choi *et al.* 2021). Noteworthy, in recent years, the integration of UV-curing technology and surface hydrophobic modification has become a research hotspot (Cui *et al.* 2022; Huang *et al.* 2022). For example, Periolatto and Ferrero (2015) combined self-assembly and UV-curing technology to prepare washable cotton fibers, and the modified fabric still exhibited a certain hydrophobic effect as well as good softness and permeability.

With the development of combined coating technology, hybrid coatings can be obtained through a dual curing process, in which the sol–gel reaction of inorganic precursors is combined with the photopolymerization of reactive monomers/oligomers (Kesmez 2019). This photopolymerization or UV-curing process involves low energy consumption, rapid curing speed, non-requirement of organic solvents, and is more environmentally friendly, durable, and does not require secondary processing compared with traditional surface spraying of resin paints. Chitosan (CS) is a deacetylation product of chitin, which is the second most abundant natural polysaccharide after cellulose and is considered an eco-friendly biomaterial. Several studies have been dedicated to enhancement of the low mechanical, thermal, gas barrier, and water resistance properties of these films (Mardyukov and Studer 2013). Moreover, the product is characterized by better processing technology. At present, it is applied only for hydrophobic treatment of fabric surface (Banerjee *et al.* 2019; Pakdel *et al.* 2022). However, the surface functionalization of biocomposites, in particular, straw-based biocomposites has rarely been reported to date.

In this study, an easy and effective coating method was used to enhance the dimensional stability of straw-based biocomposites by sol–gel method combined with UV-curing technology. The effects of key UV-curable process, as well as the hydrolysis time, photoinitiator dosage, and CS dosage on the dimensional stability of straw-based biocomposites, were systematically evaluated. The optimum preparation parameters were obtained *via* the Box–Behnken experimental design to provide economic, environmentally friendly, and moisture-proof treatment ideas for broadening the application range of straw-based composites.

EXPERIMENTAL

Materials and Methods

Corn straw was obtained from Anda (Heilongjiang province, China), and the skins were separated using a skin separator (XZ2020, Xingtai Hengkong Jiacheng Machinery Manufacturing Development, China). The skins were reduced to particles using a flaker (FW-100 high-speed shredder, Changzhou, China). The corn stalk particles (CP) were dried to a moisture content of 5% and then filtered through 40-mesh to 60-mesh for separation. The average chemical compositions of CP were determined to be 17.7% lignin, 45.6% cellulose, 24.5% hemicelluloses, 9.3% extractives, and 2.9% ash. Lignosulfonate was obtained from Shenyang Xingzhenghe Chemical Company (Shenyang, China). All other chemicals were of analytical grade.

The straw-based biocomposites were self-made in the laboratory, following the preparation process reported in the literature (Li *et al.* 2023). Briefly, CP were mixed with modified lignosulfonate binder at different proportions in a SHR-10A high-speed blender (Zhangjiagang Yunfan Machinery Co., Ltd., Zhangjiagang, China). The mixed particles were then fixed into a mat of a forming box with dimension of 250 mm × 250 mm, and then hot-pressed into biocomposites. The target density of all biocomposites was determined as 0.8 ± 0.03 g/cm^3 with a target thickness of 5 mm, and then the samples were hot-pressed at 160 °C under 3.0 MPa of pressure for 5 min. 3-(Trimethoxy-silyl) propyl methacrylate (MEMO), polyvinyl alcohol (PVOH), and 2-hydroxy-2-methyl-1-phenylpropan-1-one (Darocur 1173) were obtained from Aladin Reagent Co., Ltd. (Shanghai, China). The CS and sterile deionized water were obtained from Sigma-Aldrich Company (Shanghai, China).

Preparation of UV-curable sol

Preparation of UV-curable sol was inspired by the literature (Periolatto and Ferrero 2015; Li and Li 2018). The modified processes were as follows, a PVOH solution was firstly prepared by dissolving PVOH (4 g) in deionized water (100 mL) at 75 °C for 2 h under magnetic stirring. Second, using MEMO as the sol–gel precursor, a certain amount of anhydrous ethanol was added, the contents were stirred at room temperature for 10 min, and PVOH solution was added slowly. After ultrasonic hydrolysis at 40 °C for a certain time, sol was formed. A certain amount of photoinitiator was added, the contents were stirred for 24 h, and dried at 70 °C until the solid content was 30 wt%, which resulted in the formation of UV-curable sol.

Fabrication of MEMO/PVA-coated straw-based biocomposites

Next, the UV-curable sol was coated on the surface of the straw-based biocomposites, the coating amount was 0.1 g/cm^2, and it was cured in an intelligent UV-curing box for 15 min. The effects of hydrolysis time, Darocur 1173 dosage, and CS dosage on the dimensional stabilities of the prepared biocomposites were systematically studied.

Characterization and Experimental Design

Properties of straw-based biocomposites

According to GB/T 17657 (2022), the test samples were cut into dimensions of 200 mm × 50 mm for the modulus of rupture (MOR) and modulus of elasticity (MOE) tests, and into 50 mm × 50 mm for the internal bonding strength (IB) test. A loading speed of 5 mm/min was selected for the MOR and the MOE tests and 2 mm/min for the IB test. For the 24-h thickness swelling (TS), the samples with dimensions of 50 mm × 50 mm were obtained. The specimens were first immersed in water at 20 ± 1 °C and then their thickness and weight changes were measured after 24 h. Moisture resistance (MR) was measured by three cycles of test treatment, where each cycle included cold water soaking, freezing, and drying. After cyclic treatment, IB_{MR} and TS_{MR} were measured by rebalancing for 24 h. For each test, the biocomposites were cut into three test samples after conditioning at 20 ± 2 °C and 65 ± 5% relative humidity (RH).

The load-bearing particleboard properties of GB/T 4897 (2015) were followed as MOR ≥ 14 MPa, MOE ≥ 1900 MPa, IB ≥ 0.45 MPa, 24-h TS ≤ 22%, IB_{MR} ≥ 0.18 MPa, and TS_{MR} ≤ 20%. The IB_{MR} and TS_{MR} were used as the dependent responses to discuss the effect of key UV-curable process on the dimensional stability of the straw-based biocomposites.

ATR-FTIR spectroscopy and SEM characterization

Attenuated total reflectance-Fourier transform infrared (ATR-FTIR) spectroscopy results of straw-based biocomposites before and after the application of UV-curable coating were obtained using a spectrometer (Nicolet Nexus 670, ThermoFisher Scientific, Madison, WI, USA). The spectra were recorded at wavelengths ranging from 4,000 to 500 cm^{-1}. Each sample was scanned 40 times at resolution of 4 cm^{-1}. Scanning electron microscopy (SEM) analysis was conducted to characterize the morphological changes in straw-based biocomposites before and after the application of UV-curable coating using a scanning electron microscope (Sirion 200, FEI Company, Hillsboro, OR, USA).

Box–Behnken experimental design (BBD)

The BBD was applied using Design-Expert 8.0.6 software (Stat-Ease Inc., Minneapolis, MN, USA). The three major parameters including the hydrolysis time (X_A), Darocur 1173 dosage (X_B), and CS dosage (X_C) were independent variables, and the response variables were IB_{MR} and TS_{MR}. A total of 17 experiments were carried out in Table 1. Data were expressed from three replicates along with their coefficient of standard deviation (SD).

Table 1. Experimental Design of Coded Factors and Results of Box–Behnken Design for Dimensional Stability of Straw-Based Biocomposites

Coded	Factors			Range and Levels		
				Low (−1)	Medium (0)	High (1)
A	Hydrolysis Time (min)			20	30	40
B	Darocur 1173 Dosage (wt%)			2	4	6
C	CS Dosage (wt%)			1	2	3
Run	Factors			Density (g/cm^3)	IB_{MR} (MPa)	TS_{MR} (%)
	A	B	C			
1	0 (30)	0 (4)	0 (2)	0.80 ± 0.02	0.32 ± 0.013	18.5 ± 0.28
2	0 (30)	0 (4)	0 (2)	0.80 ± 0.03	0.34 ± 0.015	18.2 ± 0.26
3	0 (30)	1 (6)	−1 (1)	0.79 ± 0.02	0.17 ± 0.014	25.6 ± 0.32
4	0 (30)	0 (4)	0 (2)	0.78 ± 0.02	0.35 ± 0.015	18.4 ± 0.30
5	−1 (20)	−1 (2)	0 (2)	0.79 ± 0.03	0.09 ± 0.014	33.2 ± 0.33
6	−1 (20)	0 (4)	−1 (1)	0.81 ± 0.02	0.06 ± 0.012	31.9 ± 0.32
7	0 (30)	0 (4)	0 (2)	0.82 ± 0.01	0.37 ± 0.012	18.4 ± 0.26
8	1 (40)	1 (6)	0 (2)	0.82 ± 0.01	0.19 ± 0.014	26.4 ± 0.28
9	0 (30)	−1 (2)	1 (3)	0.80 ± 0.03	0.28 ± 0.015	21.3 ± 0.30
10	1 (40)	0 (4)	1 (3)	0.78 ± 0.04	0.26 ± 0.013	20.1 ± 0.27
11	−1 (20)	0 (4)	1 (3)	0.79 ± 0.02	0.34 ± 0.016	18.5 ± 0.25
12	0 (30)	−1 (2)	−1 (1)	0.80 ± 0.03	0.07 ± 0.011	29.8 ± 0.32
13	1 (40)	0 (4)	−1 (1)	0.82 ± 0.01	0.20 ± 0.013	23.4 ± 0.34
14	0 (30)	1 (6)	1 (3)	0.81 ± 0.01	0.30 ± 0.016	18.9 ± 0.28
15	1 (40)	−1 (2)	0 (2)	0.82 ± 0.02	0.10 ± 0.012	28.9 ± 0.24
16	−1 (20)	1 (6)	0 (2)	0.80 ± 0.01	0.13 ± 0.011	28.0 ± 0.30
17	0 (30)	0 (4)	0 (2)	0.78 ± 0.03	0.35 ± 0.012	18.0 ± 0.26

RESULTS AND DISCUSSION

Data Analysis and Regression Models

The ANOVA p-values are presented using Design-Expert 8.0.6 software in Table 2. All p-values below 0.05 revealed significant model terms, while values above 0.05 indicated insignificant model terms (Alslaibi *et al.* 2013). Moreover, p-values below 0.0001 indicated that all models of mechanical properties were significant and there was only a 0.01% chance that such values could occur due to noise.

Table 2. ANOVA for p-Values of Parameters and their Interactions

Response	Model	X_A	X_B	X_C	$X_A X_B$	$X_A X_C$	$X_B X_C$	X_A^2	X_B^2	X_C^2
IB	< 0.001	0.0128	0.0004	< 0.001	0.1143	< 0.001	0.0235	< 0.001	< 0.001	0.0055
TS	< 0.001	< 0.001	< 0.001	< 0.001	0.0040	< 0.001	0.0261	< 0.001	< 0.001	0.8772[ns]

[ns] Not significant

The regression equation for IB was as follows:

IB = 0.35 + 0.016X_A + 0.031X_B + 0.085X_C + 0.012X_AX_B − 0.055X_AX_C − 0.20X_BX_C − 0.11X_A^2 − 0.12X_B^2 − 0.031X_C^2

Table 2 shows that only X_AX_B was not significant. The F-value of 112.62 indicates that the model was significant. A p-value < 0.05 is indicative of the significance of the model terms. The high value of R^2 (0.9931) indicates a high level of model fitting. All predicted R^2 values (0.9974) agreed well with the adjusted R^2 values (0.9843). The lack of fit F-value of 0.025 indicates that the lack of Fit is not significant relative to the pure error. The low coefficient variance (CV% = 6.01) confirmed the accuracy and reliability of the experimental values in the regression model of IB_{MR}.

Simultaneously, the regression equation of TS is as follows:

TS = 18.31 − 1.55X_A − 1.79X_B − 3.94X_C + 0.67X_AX_B + 2.43X_AX_C + 0.45 X_BX_C + 5.14X_A^2 + 5.67X_B^2 − 0.081X_C^2.

Only X_C^2 was not significant in Table 2. The F-value of 502.49 presents that the model is significant. A p-value < 0.05 is indicative of the significance of the model terms. A high level of model fitting was indicated by the high value of R^2 (0.9985). All predicted R^2 values (0.9802) agreed well with the adjusted R^2 values (0.9965). Values of adequate precision greater than four are appropriate. The lack of fit F-value of 4.65 indicates that the lack of fit is not significant relative to the pure error. The low CV% of 1.37 confirmed the accuracy and reliability of the experimental values in the regression model of TS_{MR}.

Response Surface Interaction Analysis

The three-dimensional (3D) response surface and contour plots for IB_{MR} are shown in Fig. 1. The 3D response surface plot and the 2D response contour plot provide a visual interpretation of the interaction between two independent variables. The 3D response surface diagram shows the interaction between independent variables and response variables. The 2D response contour map can not only explain the interaction between independent variables, but also reflect the importance of the interaction between variables. That is, the circular response contour plot shows that the interaction between the corresponding variables is negligible, whereas the elliptic response contour plot shows that significant interaction occurs between the corresponding variables (Guo *et al.* 2010; Zhang *et al.* 2022).

Figure 1 demonstrates that the interaction effect between the hydrolysis time (X_A) and CS dosage (X_C) was greater than that between different Darocur 1173 dosage (X_B) and CS dosage (X_C). In turn, the interaction effect between different Darocur 1173 dosages (X_B) and CS dosages (X_C) were greater than that between different hydrolysis time (X_A) and Darocur 1173 dosage (X_B), *i.e.*, $X_AX_C > X_BX_C > X_AX_B$.

Figure 2 illustrates that the interaction effect between the hydrolysis time (X_A) and CS dosage (X_C) was greater than that between different hydrolysis time (X_A) and Darocur 1173 dosage (X_B). In turn, the interaction effect between different hydrolysis time (X_A) and Darocur 1173 dosage (X_B) was greater than that between different Darocur 1173 dosage (X_B) and CS dosage (X_C), *i.e.*, $X_AX_C > X_AX_B > X_BX_C$.
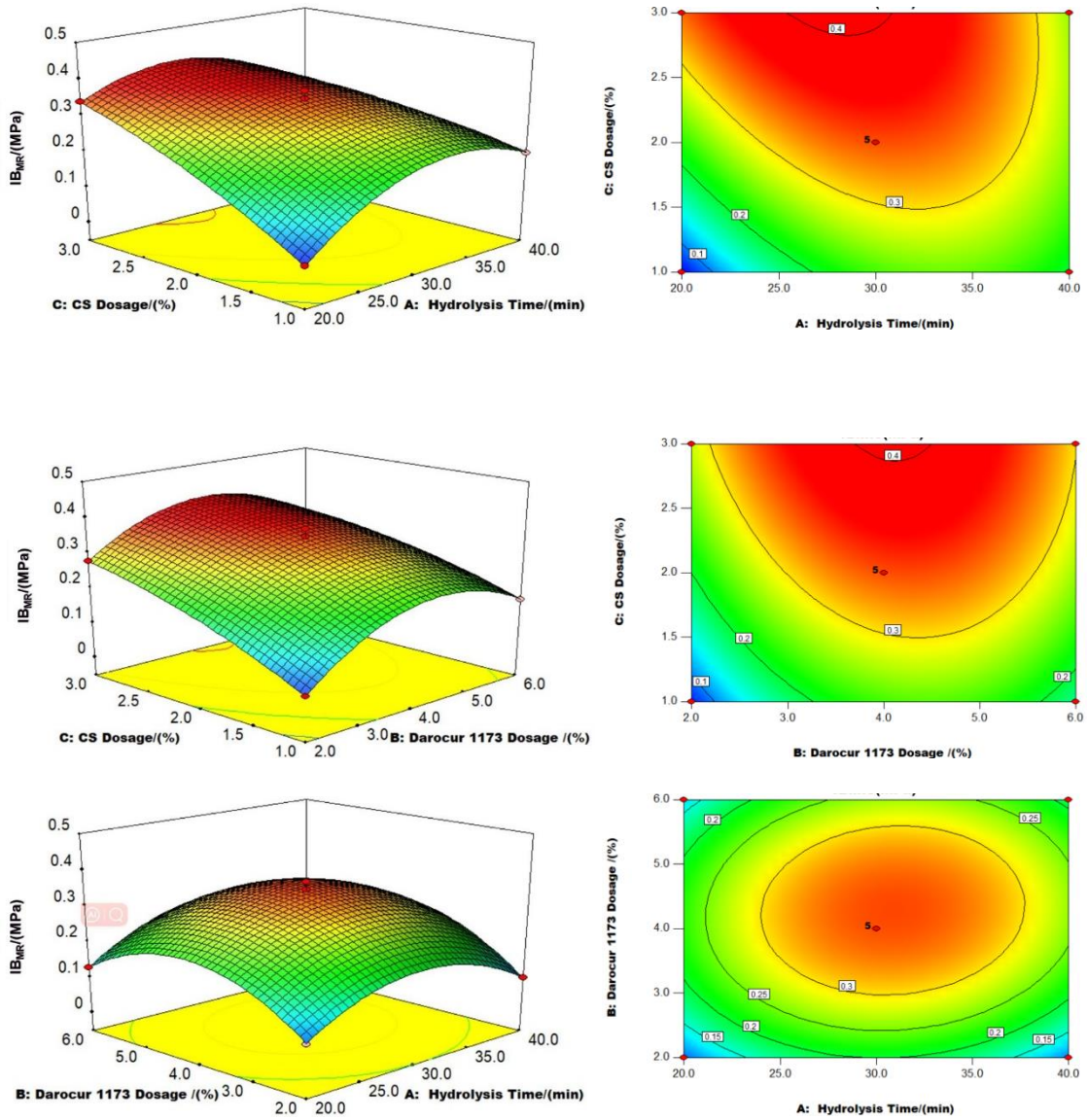
Fig. 1. Response surface plots and response contour plots showing the interaction effect of hydrolysis time (X_A), Darocur 1173 dosage (X_B), and CS dosage (X_C) on IB_{MR}
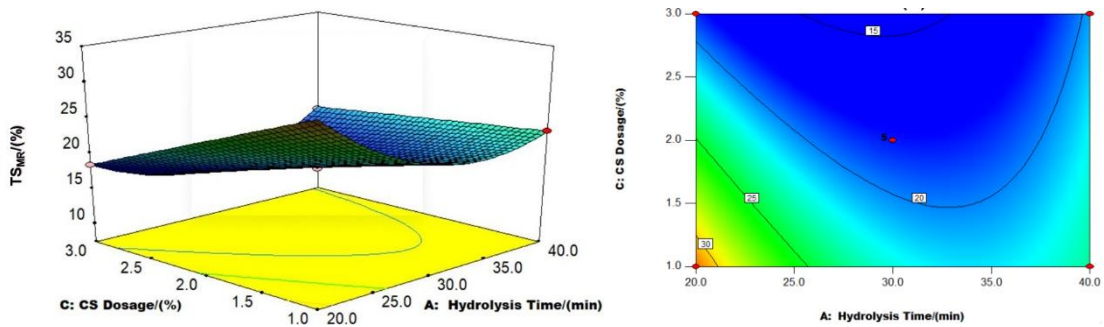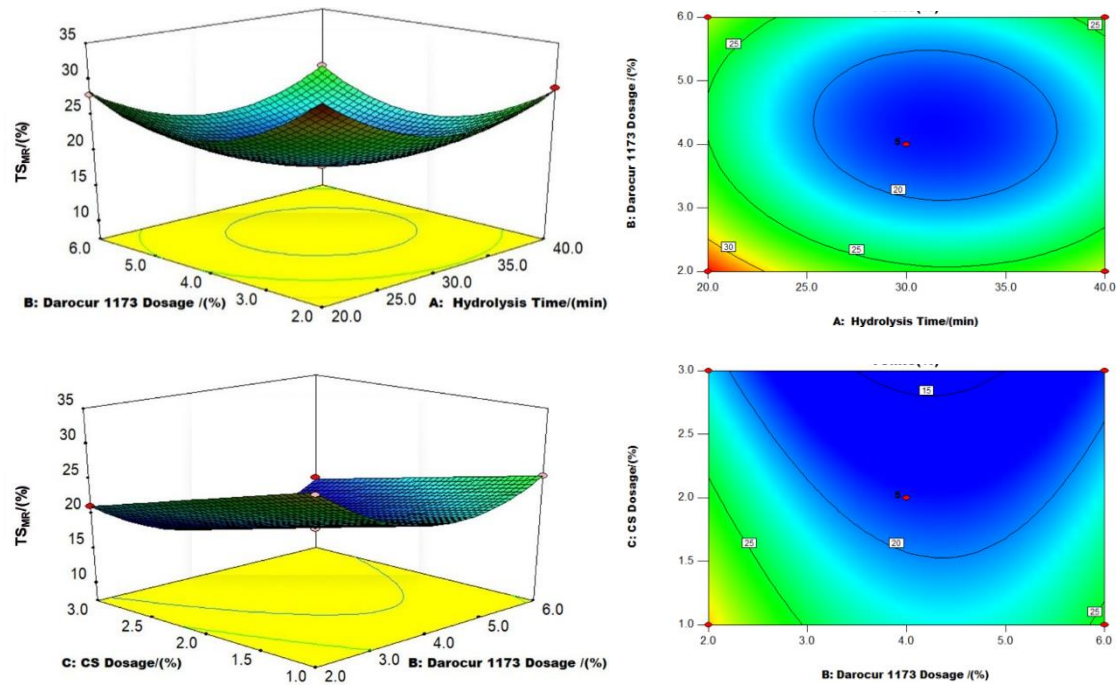
Fig. 2. Response surface plots and response contour plots showing the interaction effect of hydrolysis time (X_A), Darocur 1173 dosage (X_B), and CS dosage (X_C) on TS_{MR}

Optimization and Verification Experiment

The main objective was to figure out the optimal preparation conditions that could aid in providing maximum value of IB_{MR} and minimum value of TS_{MR}. The predicted experimental conditions with the highest desirability were selected for verification. Based on the optimization analysis, validation experiments were performed following the same method that was performed under the optimum conditions, *i.e.*, hydrolysis time of 31.9 min; Darocur 1173 dosage of 4.5%; and CS dosage of 2.7%. Under these conditions, the optimum values of manufacturing factors and their responses of straw-based biocomposites before and after UV curing were obtained (Table 3).

Table 3. The Optimum Solution Suggested by Using Design Expert Software

Sample		Thickness (mm)	Density (g/cm^3)	Mechanical Property				Moisture Resistance after Cycle Test	
				MOR (MPa)	MOE (GPa)	IB (MPa)	24-h TS (%)	IB_{MR} (MPa)	TS_{MR} (%)
Predicted Data		5.2	0.82	-	-	-	-	0.38	15.8
Experim. Data	C-MEMO/PVA-coated	5.2	0.82	33.5	3542	1.12	13.4	0.34	17.3
	Untreated surface	5.2	0.82	31.2	3309	0.97	19.8	0.20	22.5
GB/T 4897 (2015) load-bearing particleboard		≤6	0.65 to 0.88	14	1900	0.45	22	0.18	20

The results show that the mechanical properties of the biocomposites after surface hydrophobic modification improved to a certain extent, with the increase in MOR, MOE, and IB by 7.3%, 7.0%, and 15.5%, respectively, and 24-h TS decreased 32.3%. Furthermore, IB_{MR} increased 70.0% and TS_{MR} decreased 23.1% after cyclic test, which fully meets the requirements of furniture particleboard under the humid state of GB/T 4897 (2015) and can be directly applied to public humid-environment applications such as bath furniture and bathroom partition.

ATR-FTIR Spectroscopy Analyses

The ATR-FTIR spectra of straw-based boards before and after UV curing are shown in Fig. 3. The strength of the –OH vibration peak at 3292 to 3337 cm^{-1} and the C–N stretching vibration peak at 1415 cm^{-1} increased, while that of the methene C–H vibration peak at 2890 to 2938 cm^{-1} decreased. The absorbance band at 1640 cm^{-1} assigned to the stretching vibration of the C–C bond approached zero, which indicates that the polymerization of the UV-cured film (Periolatto *et al.* 2013) had occurred. The new absorbance bands of Si–C, Si–O–Si, C–O, and C–H bonds were located at 845, 1076, 1730, and 2930 cm^{-1}, respectively. For example, the Si–O–Si absorbance peak at 1076 cm^{-1} indicates the condensation reaction of hydrolyzed silane, which demonstrates the formation of SiO$_2$ in MEMO/PVA coating (Li and Li 2018).

For improving the stability of MEMO/PVA coating, the effect of additive CS on the formation of UV-cured film on the surface of straw-based biocomposite was further accessed. After the addition of CS, the C–N stretching vibration peak at 1415 cm^{-1} enhanced, indicating that CS promoted the cross-linking of MEMO/PVA on the surface of biocomposite to form CS-MEMO/PVA (Sims *et al.* 2022).
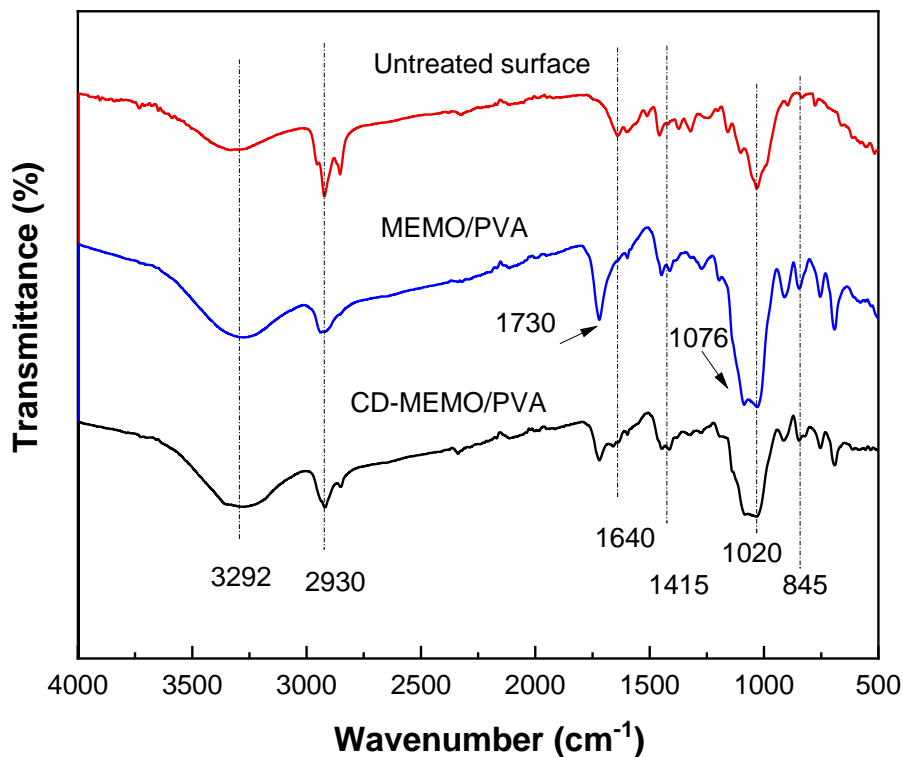
Fig. 3. ATR-FTIR spectra of straw-based boards before and after UV curing

The possible formation mechanism of the CS-MEMO/PVA-modified composite is shown in Fig. 4. The strategy involves the activation of MEMO by hydrolyzing the alkoxy groups off, thereby forming the reactive silanol groups, similar to the hydrolysis process of organosilane (Li *et al.* 2017). Then, the reactive silanol reacts with the hydroxyl groups, which undergo condensation reaction to form macromolecular networks. The differences of surface morphologies between uncoated biocomposite and CS-MEMO/PVA-modified biocomposite indicate that the MEMO successfully created a chemical bridge between the particles at each interface.
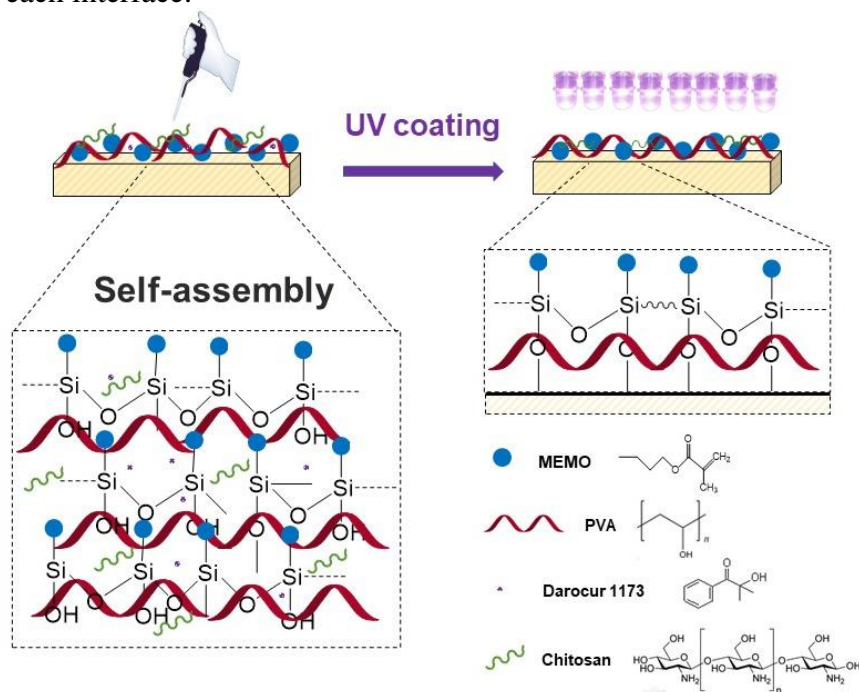
Fig. 4. Schematics showing the formation mechanism of the CS-MEMO/PVA-coated straw-based biocomposites

Surface Morphologies

The SEM images of uncoated biocomposite, MEMO/PVA-coated biocomposite, and CS-MEMO/PVA-modified biocomposite are shown in Fig. 5.
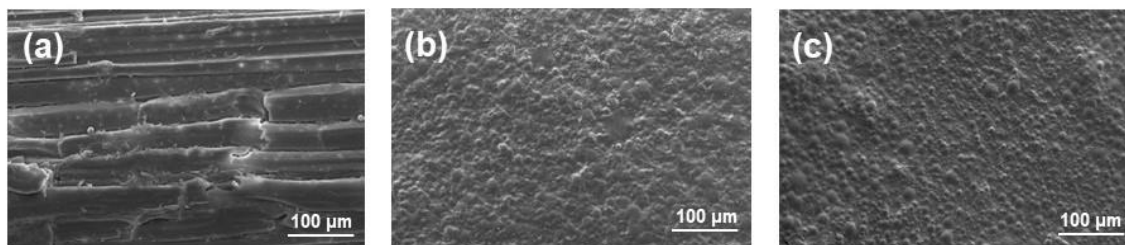
Fig. 5. SEM images of straw-based biocomposites before and after UV curing (a: untreated surface; b: MEMO/PVA-coated surface; and c: CS-MEMO/PVA-coated surface)

The figure clearly illustrates the dispersion of the SiO_2 particles in non-porous hydrophobic MEMO/PVA hybrid film (Fig. 5b). More interestingly, the glossy spherical particles were arranged in a fish-scale shape with scales closely linked with each other, and no agglomeration occurred in CS-MEMO/PVA hybrid film (Fig. 5c). Such arrangement is

conducive to the formation of hydrophobic network structure between the particles at each interface (Li and Li 2018).

CONCLUSIONS

1. The three major parameters including the hydrolysis time, 2-hydroxy-2-methyl-1-phenylpropan-1-one (Darocur 1173) dosage, and chitosan (CS) dosage were independent variables, and the response variables were internal bonding strength (IB_{MR}) and thickness swelling (TS_{MR}). All variables and interactions between each other were significant for IB_{MR} and TS_{MR}.

2. The response surface methodology based on the Box–Behnken design was employed to obtain the optimal conditions, *i.e.*, hydrolysis time of 31.9 min; Darocur 1173 dosage of 4.5%; and CS dosage of 2.7%. The optimum modulus of rupture (MOR), modulus of elasticity (MOE), IB, 24-h TS, IB_{MR} and, TS_{MR} of the biocomposites complied with the requirement of load-bearing particleboard, which were 33.5 MPa, 3542 MPa, 1.12 MPa, 13.4%, 0.34 MPa and 22.5%, respectively.

3. The TS_{MR} of C-MEMO/PVA-coated straw-based biocomposites resulted in ~23.1% reduction in dimensional stability without any significant decline in the mechanical properties when compared with those before UV curing. C-MEMO/PVA-coated straw-based biocomposites can be directly applied to public humid-environment applications such as bath furniture and bathroom partition.

4. The attenuated total reflection – Fourier transform infrared (ATR-FTIR) spectroscopy and scanning electron microscopy (SEM) results demonstrated that the C-MEMO/PVA coating formed a hydrophobic macromolecular network on straw-based biocomposites. Chitosan promoted the cross-linking of non-porous hydrophobic MEMO/PVA on the surface of biocomposite.

ACKNOWLEDGMENTS

REFERENCES CITED

Alslaibi, T. M., Abustan, I., Ahmad, M. A., and Foul, A. A. (2013). "Cadmium removal from aqueous solution using microwaved olive stone activated carbon," *Journal of Environmental and Chemical Engineering* 1(3), 589-599. DOI: 10.1016/j.jece.2013.06.028

Banerjee, S. L., Potluri, P., and Singha, N. K. (2019). "Antimicrobial cotton fibre coated with UV cured colloidal natural rubber latex: A sustainable material," *Colloids and Surfaces A-Physicochemical and Engineering Aspects* 566, 176-187. DOI: 10.1016/j.colsurfa.2019.01.018

Choi, S. H., Kim, D. H., Kim, S., Kim, W. Y., Kim, S., and Cho, Y. T. (2021). "Tulip-shaped pattern imprinting for omni-phobic surfaces using partially cured photopolymer," *Applied Sciences-Basel* 11(4), article 1747. DOI: 10.3390/app11041747

Cui, Y., Wei, B., Wang, Y., Guo, X., Xiao, J., Li, W., Pang, A., and Bai, Y. (2022). "Fabrication of UV/moisture dual curing coatings based on fluorinated polyoxetanes for anti-fouling applications," *Progress in Organic Coatings* 163, article ID 106656. DOI: 10.1016/j.porgcoat.2021.106656

Dong, X., Ren, J., Duan, Y., Wu, D., Lin, L., Shi, J., Jia, R., Xu, X., and He, X. (2022). "Preparation and properties of green UV-curable itaconic acid cross-linked modified waterborne polyurethane coating," *Journal of Applied Polymer Science* 139, article e52042. DOI: 10.1002/app.52042

Gao, L. K., Lu, Y., Zhan, X. X., Li, J., and Sun, Q. F. (2015). "A robust, anti-acid, and high-temperature-humidity-resistant superhydrophobic surface of wood based on a modified TiO_2 film by fluoroalkyl silane," *Surface and Coatings Technology* 262, 33-39. DOI: 10.1016/j.surfcoat.2014.12.005

Gao, X. M., Wang, M. K., and He, Z. W. (2023). "Superhydrophobic wood surfaces: recent developments and future perspectives," *Coatings* 13(5), article 877. DOI: 10.3390/coatings13050877

GB/T 4897 (2015). "Particleboard," Standardization Administration of China, Beijing, China.

GB/T 17657 (2022). "Methods of evaluating the properties of wood-based panels and surface decorated wood-based panels," Standardization Administration of China, Beijing, China.

Ghazali, S. K., Adrus, N., Majid, R. A., Ali, F., and Jamaluddin, J. (2021). "UV-LED as a new emerging tool for curable polyurethane acrylate hydrophobic coating," *Polymers* 13(4), article 487. DOI: 10.3390/polym13040487

Guo, X., Zou, X., and Sun, M. (2010). "Optimization of extraction process by response surface methodology and preliminary characterization of polysaccharides from *Phellinus igniarius*," *Carbohydrate Polymers* 80(2), 344-349. DOI: 10.1016/j.carbpol.2009.11.028

Huang, J., Yang, M., Zhang, H., and Zhu, J. (2021). "Solvent-free fabrication of robust superhydrophobic powder coatings," *ACS Applied Materials and Interfaces* 13(1), 1323-1332. DOI: 10.1021/acsami.0c16582

Huang, L., Wang, Y., Wei, Z., Han, X., Mo, Q., Wang, X., and Li, Y. (2022). "Synthesis and optimization of a free-radical/cationic hybrid photosensitive UV curable resin using polyurethane acrylate and graphene oxide," *Polymers* 14(10), article 1959. DOI: 10.3390/polym14101959

Kesmez, O. (2019). "Preparation of UV-curable hybrid films *via* sol-gel synthesis for hydrophobic surface applications," *Journal of Sol-Gel Science and Technology* 91(1), 1-10. DOI: 10.1007/s10971-019-05027-x

Luo, H. L., Zhang, C. Y., Xiong, G. Y., and Wan, Y. Z. (2016). "Effects of alkali and alkali/silane treatments of corn fibers on mechanical and thermal properties of its composites with polylactic acid," *Polymer Composites* 37(12), 3499-3507. DOI: 10.1002/pc.23549

Li, S. D., Bin, Y. J., Zhong, S., Wang, W. D., Sun, G. B., Zeng, Y. M., Chen, S. J., Li, Z. R., and Yuan, Y. (2023). "Two modified treatment methods for pretreated corn stalk and its composites with modified lignosulfonate," *BioResources* 18(3), 4805-4818. DOI: 10.15376/biores.18.3.4805-4818

Li, X. Q., Zhang, G. C., Ge, J. J., Qi, N., Jiang, P., Liao, K. L., and Qiao, W. L. (2017). "Organosilane film for sand migration control based on in-situ hydrolysis and polycondensation effects," *Journal of Petroleum Science and Engineering* 158, 660-671. DOI: 10.1016/j.petrol.2017.08.013

Li, Y., and Li, J. (2018). "Fabrication of reversible thermoresponsive thin films on wood surfaces with hydrophobic performance," *Progress in Organic Coatings* 119, 15-22. DOI: 10.1016/j.porgcoat.2018.02.004

Liu, S. Q., Zhu, M. J., Huang, Y. X., Yu, Y. L., Yu, W. J., and Lv, B. (2023). "A nature-inspired strategy towards superhydrophobic wood," *Journal of Materials Chemistry A* 11(47), 25875-25886. DOI: 10.1039/d3ta05013k

Mardyukov, A., and Studer, A. (2013). "Preparation of photoactive polymers and postmodification *via* nitroxide trapping under UV irradiation," *Macromolecular Rapid Communications* 34(1), 94-101. DOI: 10.1002/marc.201200595

Mathias, J. D., Alzina, A., Grédiac, M., Michaud, P., Roux, P., De Baynast, H., Delattre, C., Dumoulin, N., Faure, T., Larrey-Lassalle, P., Mati-Baouche, N., Pennec, F., Sun, S., Tessier-Doyen, N., Toussaint, E., and Wei, W. (2015). "Upcycling sunflower stems as natural fibers for biocomposite applications," *BioResources* 10(4), 8076-8088. DOI: 10.15376/biores.10.4.8076-8088

Nkeuwa, W. N., Riedl, B., and Landry, V. (2014a). "UV-cured clay/based nanocomposite topcoats for wood furniture: Part I: Morphological study, water vapor transmission rate and optical clarity," *Progress in Organic Coatings* 77(1), 1-11. DOI: 10.1016/j.porgcoat.2013.03.021

Nkeuwa, W. N., Riedl, B., and Landry, V. (2014b). "Wood surfaces protected with transparent multilayer UV-cured coatings reinforced with nanosilica and nanoclay. Part I: Morphological study and effect of relative humidity on adhesion strength," *J. Coatings Technol. Research* 11(3), 283-301. DOI: 10.1007/s11998-013-9551-x

Noor Haris, N. F., Yahaya, M. A., and Mahmud, J. (2022). "Tensile properties of silicone biocomposite reinforced with waste material (*Hevea brasiliensis* sawdust): Experimental and numerical approach," *BioResources* 17(3), 4623-4637. DOI: 10.15376/biores.17.3.4623-4637

Okuda, N., and Sato, M. (2007). "Bond durability of kenaf core binderless boards I: Two-cycle accelerated aging boil test," *Journal of Wood Science* 53(2), 139-142. DOI: 10.1007/s10086-006-0829-9

Pakdel, E., Xie, W., Wang, J., Kashi, S., Sharp, J., Zhang, Q., Varley, R. J., Sun, L., and Wang, X. (2022). "Superhydrophobic natural melanin-coated cotton with excellent UV protection and personal thermal management functionality," *Chemical Engineering Journal* 433, article ID 133688. DOI: 10.1016/j.cej.2021.133688

Periolatto, M., and Ferrero, F. (2015). "Cotton and polyester surface modification by methacrylic silane and fluorinated alkoxysilane via sol-gel and UV-curing coupled process," *Surface and Coatings Technology* 271, 165-173. DOI: 10.1016/j.surfcoat.2014.12.048

Periolatto, M., Ferrero, F., Montarsolo, A., and Mossotti, R. (2013). "Hydrorepellent finishing of cotton fabrics by chemically modified TEOS based nanosol," *Cellulose* 20(1), 355-364. DOI: 10.1007/s10570-012-9821-2

Shah, D. U. (2013). "Developing plant fibre composites for structural applications by optimising composite parameters: A critical review," *Journal of Materials Science* 48(18), 6083-6107. DOI: 10.1007/s10853-013-7458-7

Sims, C. B., Lenora, C. U., and Furgal, J. C. (2022). "Hybrid tri-cure organo-silicon coatings for monument preservation," *Coatings* 12(8), article 1098. DOI: 10.3390/coatings12081098

Tao, X., Tian, D. X., Liang, S. Q., Jiang, P., and Fu, F. (2023). "Construction of multifunctional surface to fabricate wood-derived cellulose electrothermal composites with flame retardant and hydrophobic performance for harsh operating conditions," *Industrial Crops and Products* 202, article ID 117079. DOI: 10.1016/j.indcrop.2023.117079

Wang, Y., Tang, Z. W., Lu, S. C., Zhang, M., Liu, K., Xiao, H., Huang, L. L., Chen, L. H., Wu, H., and Ni, Y. H. (2020). "Superhydrophobic wood grafted by poly(2-(per-fluorooctyl)ethyl methacrylate) via ATRP with self-cleaning, abrasion resistance and anti-mold properties," *Holzforschung* 74(8), 799-809. DOI: 10.1515/hf-2019-0184

Yavuz, H. (2023). "Evaluation of blue *Cupressus arizonica* cone in automotive brake pad biocomposite," *BioResources* 18(3), 5182-5197. DOI: 10.15376/biores.18.3.5182-5197

Yuan, Y., Guo, M. H., and Liu, F. Y. (2014). "Preparation and evaluation of green composites using modified ammonium lignosulfonate and polyethylenimine as a binder," *BioResources* 9(1), 836-848. DOI: 10.15376/biores.9.1.836-848

Yuan, Y., Sidan, L., Feng, J., Guinan, S., Lei, Y., and Weidong, W. (2019). "Dimensional stability improvement of corn stalk biocomposites using two-part lignin-derived binder optimized with response surface methodology," *BioResources* 14(3), 5923-5942. DOI: 10.15376/biores.14.3.5923-5942

Zhang, H. L., and Guo, Z. G. (2023). "Recent advances in self-healing superhydrophobic coatings," *Nano Today* 51, article ID 101933. DOI: 10.1016/j.nantod.2023.101933

Zhang, Y. L., He, L., Li, Q., Cheng, J. W., Wang, Y. B., Zhao, J. C., Yuan, S. F., Chen, Y. J., and Shi, R. (2022). "Optimization of ultrasonic-assisted deep eutectic solvent for the extraction of polysaccharides from *Indocalamus tessellatus* leaves and their biological studies," *Sustainable Chemistry and Pharmacy* 30, article ID 100855. DOI: 10.1016/j.scp.2022.100855